photonics

MDPI

Article

Long-Cavity M-Plane GaN-Based Vertical-Cavity Surface-Emitting Lasers with a Topside Monolithic Curved Mirror †

Nathan C. Palmquist [1,*], Ryan Anderson [1], Jared A. Kearns [1], Joonho Back [2], Emily Trageser [1], Stephen Gee [1], Steven P. Denbaars [1,2] and Shuji Nakamura [1,2]

1 Materials Department, University of California, Santa Barbara, CA 93106, USA; randerson@ucsb.edu (R.A.); etrageser@ucsb.edu (E.T.); stephengee@ucsb.edu (S.G.); spdenbaars@ucsb.edu (S.P.D.); snakamura@ucsb.edu (S.N.)

2 Electrical and Computer Engineering Department, University of California, Santa Barbara, CA 93106, USA; joonho@ucsb.edu

* Correspondence: palmquist@ucsb.edu

† This paper is an extended version of our paper published in Proceedings of the Gallium Nitride Materials and Devices XVIII; SPIE, 15 March 2023; Volume 12421, p. 127–135.

Abstract: We report long-cavity (60.5 λ) GaN-based vertical-cavity surface-emitting lasers with a topside monolithic GaN concave mirror, a buried tunnel junction current aperture, and a bottomside nanoporous GaN distributed Bragg reflector. Under pulsed operation, a VCSEL with a 9 μm aperture had a threshold current density of 6.6 kA/cm^2, a differential efficiency of 0.7%, and a maximum output power of 290 μW for a lasing mode at 411 nm and a divergence angle of 8.4°. Under CW operation, the threshold current density increased to 7.3 kA/cm^2, the differential efficiency decreased to 0.4%, and a peak output power of 130 μW was reached at a current density of 23 kA/cm^2.

Keywords: GaN VCSEL; tunnel junction; nanoporous GaN DBR

check for updates

Citation: Palmquist, N.C.; Anderson, R.; Kearns, J.A.; Back, J.; Trageser, E.; Gee, S.; Denbaars, S.P.; Nakamura, S. Long-Cavity M-Plane GaN-Based Vertical-Cavity Surface-Emitting Lasers with a Topside Monolithic Curved Mirror †. *Photonics* **2023**, *10*, 646. https://doi.org/10.3390/photonics10060646

Received: 10 May 2023
Revised: 1 June 2023
Accepted: 1 June 2023
Published: 3 June 2023

1. Introduction

GaN-based vertical-cavity surface-emitting lasers (GaN-VCSELs) are attracting broad interest due to their low threshold currents, circular beam profiles, 2D arraying capabilities, and capability for high-frequency operation, thus promoting their applications in lighting and displays, communications, and sensing, among others [1]. While a majority of prior GaN-VCSEL demonstrations have utilized short to medium cavities (effective cavity length L_{eff} < 3 μm) [2–9], recent long-cavity demonstrations (L_{eff} > 10 μm) from Sony have been shown to provide high thermal stability, low threshold currents, and high output powers [10]. Until recently, this design held performance records for output power (15.4 mW) [11], threshold current (0.25 mA) [12], and wall-plug efficiency (WPE, 13.4%) [13], while reporting device yields above 90%. This design accomplishes this impressive performance by extending the cavity length and decreasing the longitudinal mode spacing such that there is always a resonant mode near the center of the gain peak, even as the gain peak has shifted due to self-heating. Lasers based on this design achieve lateral mode confinement within the long cavity by incorporating a curved III-nitride lens that is etched onto the bottom side of a polished substrate [14]. The curved lens minimizes the diffraction loss that would otherwise occur in long cavities [15]. As the cavity length increases for planar cavities with fixed mirror diameters, so does the diffraction loss; the typical gain of GaN QWs is approximately 1% per pass, so diffraction loss can quickly deteriorate device performance for cavities larger than 10 μm. However, converting one of the planar distributed Bragg reflectors (DBRs) into a curved DBR mirror is known to provide a stable resonator that forms a beam waist on the planar side, thereby minimizing diffraction loss. By confining the lateral mode in this way, the beam waist and propagation throughout the cavity are primarily determined by the cavity length (L) and the radius of curvature (ROC) of the mirror.

The design demonstrated by Hamaguchi et al. prioritized low-threshold conditions by placing the active region at the beam waist (100 nm from the planar mirror) and minimizing the aperture size. However, to form their lens, they had to polish the substrate down to a thickness of approximately 20 µm, thus increasing processing complexity. Additionally, placing the mirror on the bottom of the substrate requires backside alignment. It is beneficial to place the lens on top of the VCSEL cavity without needing to lap or polish the substrate down to the desired cavity thickness. For the bottomside mirror, an epitaxial option would remove the necessity for substrate thinning or flip-chip bonding.

Here, we present a long-cavity (Leff~60.5λ) m-plane GaN-VCSEL with a topside monolithic GaN concave mirror, a buried tunnel junction (BTJ), and a buried planar nanoporous GaN distributed Bragg reflector (NP DBR) that lases under CW operation. The GaN mirror has a diameter of 26 µm and an ROC of 31 µm. The active region is placed approximately 6.5 µm from the planar mirror.

2. Materials and Methods

The epitaxial device structure, shown in Figure 1 and summarized in Table 1, was grown using atmospheric metalorganic chemical vapor deposition (MOCVD) on freestanding single-side polished (SSP) m-plane $(10\bar{1}0)$ substrates with an intentional 1° miscut in the $[000\bar{1}]$ direction. The epitaxial structure consisted of a 1 µm n-GaN ([Si]~2×10^{18} cm^{-3}) buffer layer grown at 1000 °C (18 nm/min); 24 pairs of alternating unintentionally doped (UID) GaN ([Si]~1×10^{16} cm^{-3}) and n+–GaN ([Si]~4×10^{19} cm^{-3}) grown at 1180 °C (50 nm/min) to form the bottomside DBR; 3860 nm of UID GaN grown at 1000 °C (45 nm/min); 2500 nm of n-GaN ([Si]~8×10^{18} cm^{-3} grown at 1000 °C (43 nm/min); 2 × 8 nm InGaN quantum wells (MQWs) designed to emit at 410 nm with 3 nm GaN barriers grown at 857 °C (6 nm/min); 5 nm UID GaN grown at 857 °C (6 nm/min); 10 nm graded p-AlGaN ([Mg]~1×10^{19} cm^{-3}) electron blocking layer (EBL) graded along the growth direction from 30% to 0% and grown at 1000 °C (6 nm/min); 80 nm p-GaN ([Mg]~1×10^{19} cm^{-3}) grown at 1000 °C (8 nm/min); and 10.5nm p++–GaN ([Mg] ~3×10^{20} cm^{-3}) grown at 1000 °C (8 nm/min). After the first growth, the samples were treated with concentrated HF and ozone before regrowing the 8 nm n++–GaN ([Si] ~1.5×10^{20} cm^{-3}) TJ layer at 825 °C (2 nm/min) via MOCVD [16]. The buried tunnel junction (BTJ) current apertures were defined by etching 30 nm through the n++/p++–GaN layers using reactive-ion etching (RIE). Then, all samples were annealed at 730 °C in a 4:1 N_2/O_2 environment for 30 min to activate the p/p++–GaN [17]. Finally, 1810 nm n-GaN ([Si]~4×10^{18} cm^{-3}) and 1700 nm UID GaN were grown at 900 °C (45 nm/min) via MOCVD.

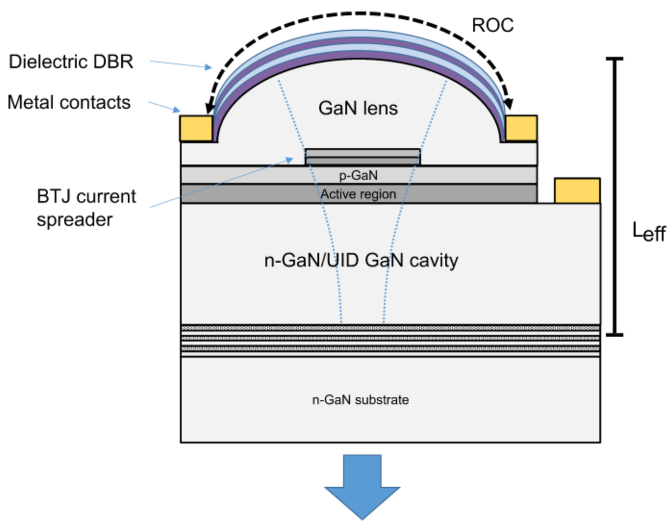

Figure 1. Schematic of the VCSEL structure with a topside curved GaN mirror.

Table 1. Epitaxial structure, doping concentrations, and absorption coefficients [18].

Growth Step	Layer	Thickness (nm)	Doping Conc. (cm^{-3})	Abs. Coeff. (cm^{-1})
	SiO_2/Ta_2O_5 DBR (16–periods)	67.5/45.5	NA	0
	GaN	1700	UID	2
3rd	n-GaN	1810	8×10^{18}	2
2nd	n++–GaN	8	1.5×10^{20}	235
1st	p++–GaN	10.5	2.5×10^{20}	180
	p-GaN	80	1×10^{19}	80
	p-AlGaN EBL	10	1×10^{19}	27
	GaN barrier	5	UID	2
	GaN/InGaN QW (2x)	3/8	UID	0
	n-GaN	2500	8×10^{18}	2
	GaN	3860	UID	2
	n+–GaN/GaN DBR (24–periods)	48.4/40.4	5×10^{19}/UID	0/0

The photoresist lenses were formed via photoresist reflow and then transferred into the upper UID/n-GaN layers using RIE [19]. Next, SiO_2 was deposited on the curved GaN lenses using plasma-enhanced chemical vapor deposition (PECVD) to act as a hard mask for subsequent processing steps. Following this, mesas were defined using RIE to allow for the p-GaN to be activated through the mesa sidewalls [20]. Next, 7 µm deep and 15 µm wide trenches were defined using RIE to etch the NP DBR. Then, all samples were annealed again at 730 C in a N_2/O_2 environment for 30 min to re-activate the BTJ through the mesa sidewalls. Next, 25 nm SiO_2 was deposited on both the top and sidewall surfaces of the mesa using atomic layer deposition (ALD) to protect the devices from the NP DBR acid etch and to provide electrical isolation [21] and sidewall passivation [22]. Next, the backside of the substrate was coated with 40 nm/450 nm Ti/Au using electron-beam evaporation, and then the samples were taped to a conductive steel holder and submerged in 0.3 M oxalic acid. A Pt wire was submerged alongside the substrate, and a bias of 2.4 V was applied for 30 h to etch the NP DBRs. Under these conditions, the n+–GaN layers of the DBR chemically reacted with the oxalic acid and formed a porous structure with pores ranging from 20 to 40 nm in diameter [23]. After the etch was completed, the bottom metal was removed with adhesive tape, and metal contacts comprised of Ti/Au (40 nm/450 nm) were deposited using electron-beam evaporation on top of the n-type GaN on the topside of the mesa and slightly overlapping the edge of the lens. Finally, a 16-period SiO_2/Ta_2O_5 dielectric DBR was deposited on the topside of the lenses using ion beam deposition (IBD).

A cross section of a completed device, taken using a focused ion beam (FIB) and imaged using scanning electron microscopy (SEM), is shown in Figure 2. Electrical characteristics were analyzed under pulsed operation with a 1000 ns pulse width and a 1% duty cycle, and under continuous-wave (CW) operation, both at room temperature (20 °C). Optical power measurements were taken by placing the sample directly on top of a Thorlabs bandpass filter centered at 410 nm with a peak transmittance of 91%; the sample and filter were placed onto a 3 mm diameter silicon photodetector (model DET36A) reverse-biased at 10 V for pulsed measurements, and placed onto a wide-area 12 mm diameter unbiased silicon photodetector (PD) for CW measurements. The bandpass filter was employed because of excess spontaneous emission present in the unfiltered LIV measurement due to the close proximity of the device to the PD, which washed out the expected LI kink. The spectrum data were acquired using an Ocean Insight spectrometer with a spectral resolution of 2 nm. The topside nearfield patterns (NFP) were taken using an optical microscope with a 20x objective lens, and the bottomside farfield patterns (FFP) were taken by placing a piece of fluorescent paper 16.5 mm below the device, which was mounted to a double-side polished (DSP) sapphire substrate. The 16.5 mm thickness included the thickness of the DSP sapphire. The resulting mode was imaged with a camera mounted at 35°.

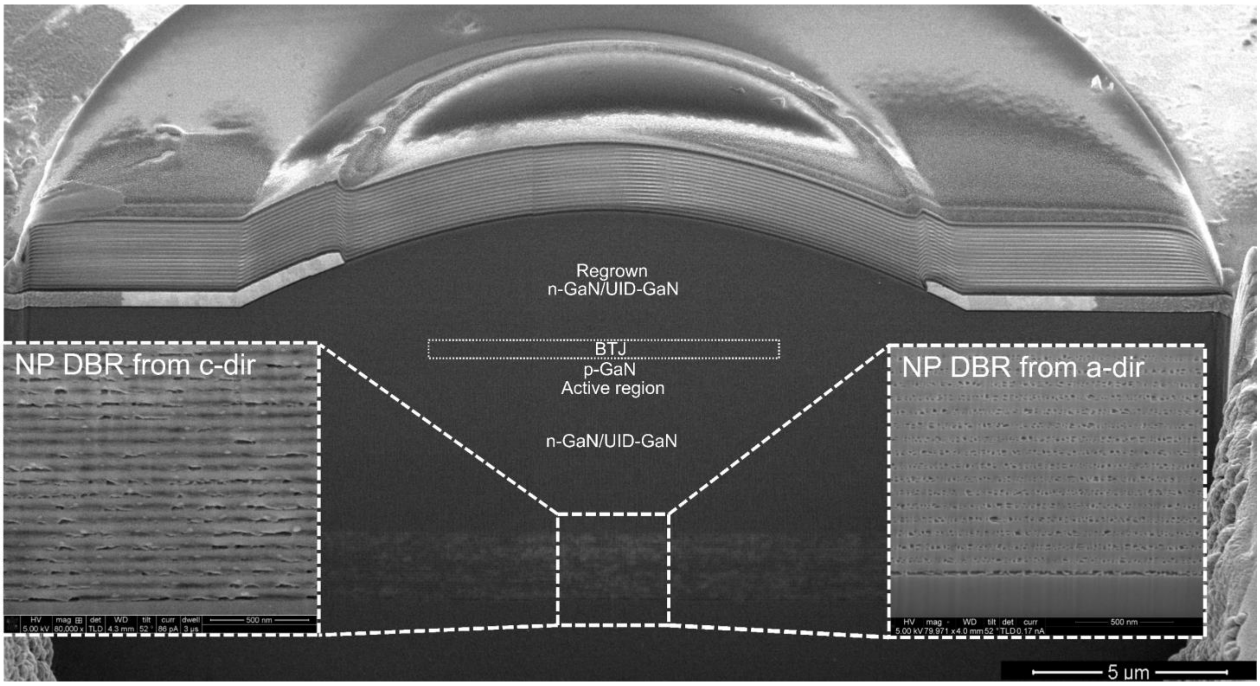

Figure 2. Cross-sectional scanning electron microscopic (SEM) image of the fabricated device structure, with the insets showing the cross sections of the NP DBR from the c- and a-directions.

3. Results and Discussion

The root-mean-square (RMS) roughness for the final regrowth surface was approximately 0.7 nm, as measured using atomic force microscopy (AFM). The fabricated devices had an effective cavity length of approximately 60.5 λ (10.7 µm) for a target emission wavelength of 410 nm. The cross-sectional SEM images of the NP DBR are shown in the insets of Figure 2, with pictures taken of the pores in the c- and a-directions. The porosity of the NP DBR was extracted by binarizing the SEM image in the a-direction and calculating the porous fraction from the known thicknesses of the individual layers. Using this method, a porosity of 29% was calculated. From there, the index of refraction of the porous layer, n_{por}, can be determined based on the volume average theory (VAT) as follows:

$$n_{por} = \left[(1-\varphi)n_{GaN}^2 + \varphi n_{air}^2\right]^{1/2} \tag{1}$$

where φ describes the porosity fraction [24]. At 410 nm, the n_{GaN} was ~2.5, leading to a calculated n_{por} of ~2.18 and creating an index contrast of 0.32. Using 1D transmission matrix method (1D TMM) simulations, the peak reflectivity of the 24-period NP DBR was 99.617%. There is inhomogeneity of the pore size observed throughout the NP DBR layers, which may lead to scattering [25]. Future studies will be conducted to further characterize the magnitude of this effect within NP DBRs for III-nitride VCSELs. Additional 1D TMM simulations were carried out to calculate the internal loss <αi>, mirror loss α_m, confinement factor $\Gamma_{xy}\Gamma_z\Gamma_{enh}$, and dielectric DBR reflectivity, which were determined to be 2.52 cm^{-1}, 1.8 cm^{-1}, 0.00117, and 99.995%, respectively [26]. The absorption coefficients listed in Table 1 are rough estimates used to guide insights into the internal loss of the structure [18].

Figure 3a shows the light-current-voltage (LIV) characteristics of a VCSEL with a 9 µm current aperture analyzed under pulsed and CW operations. Under pulsed operation, the peak total output power was 260 µW and the threshold current (J_{th}) and voltage (V_{th}) were 6.6 kA/cm^2 and 8.9 V, respectively, as determined using the linear line fitting method. Correcting for the filter transmittance gave a peak output power of 290 µW. The slope efficiency (SE) was 0.02 W/A, leading to a differential efficiency (η_d) of 0.7%. Under CW operation, J_{th} and V_{th} were 7.3 kA/cm^2 and 8.8 V, respectively, with rollover occurring at approximately 23 kA/cm^2 at a peak total power of 120 µW, or 130 µW with filter correction. The SE reduced to 0.013 W/A, resulting in a reduced η_d of 0.4%.

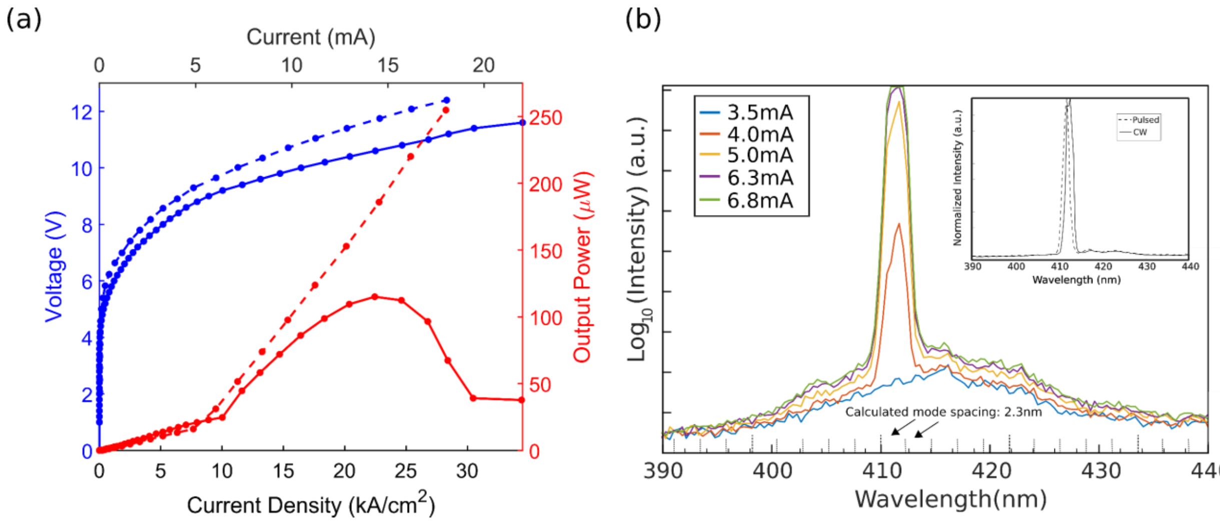

Figure 3. (**a**) LIV for pulsed (solid) and CW (dashed) operations of a VCSEL with a 9 µm current aperture. The inset features LI for pulsed (solid) and CW (dashed) operations through a Thorlabs bandpass filter. (**b**) Pulsed emission spectrum as a function of injected current. The inset shows the comparison between the pulsed and CW spectra taken at 8 mA (12.5 kA/cm^2). The arrows designate adjacent longitudinal peak positions.

The diameter of a Gaussian beam, $2\omega(z)$, at the location of the active region can be expressed using the following equation [27]:

$$2\omega(z) = 2\omega_0\sqrt{1 + (\frac{\lambda z}{n\pi\omega_0^2})^2} \quad (2)$$

where λ is the lasing wavelength and n is the index refraction. ω_0 is the beam waist radius formed at the planar mirror and can be calculated as follows:

$$\omega_0 = \sqrt{\frac{\lambda}{n\pi}\sqrt{L_{eff}R - L_{eff}^2}} \quad (3)$$

where L_{eff} is the effective cavity length and R is the ROC of the concave lens. At the active region, which is placed approximately 6.5 µm from the planar mirror, 99.7% of the Gaussian profile is contained in a 5.8 µm diameter. This was calculated by calculating the beam diameter using Equations (2) and (3), and then multiplying the result by three to account for 99.7% of the light. The result suggests that only 41% of the 9 µm current aperture is coupled to the resonant mode, and the remaining light becomes excess spontaneous emission. Additionally, there is current crowding observed around the edge of the 9 µm aperture. This non-uniformity in current distribution could lead to increased recombination at the edge of the aperture and outside of the mode, which is approximately centered over the aperture. Figure 3b shows the unfiltered spectra as a function of the injected current under pulsed operation, showing the selection of a mode centered at 411 nm that grows with the injected current. The inset of Figure 3b shows the lasing behavior at a bias of 8 mA under pulsed and CW operations, showing a minimal shift of the mode at the injected current. It should be noted that the resolution of the spectrometer (2 nm) is similar to the longitudinal-mode spacing calculated using 1D TMM modeling (2.3 nm). The arrows designate adjacent longitudinal peak positions, which are almost at the same position of the observed peak emission wavelength. Additional equipment is needed to accurately resolve the longitudinal-mode behavior.

Prior NP-DBR VCSEL demonstrations with cavity lengths of 8.9λ [28], 6λ [6], 6λ [7], and 1.5λ [29] exhibited threshold currents of 20 kA/cm^2 (pulsed), 42 kA/cm^2 (pulsed), 59 kA/cm^2 (pulsed), and 0.7 kA/cm^2 (CW), respectively. Previous curved mirror VCSEL demonstrations exhibited threshold current densities that ranged from 3.5 to 141 kA/cm^2 [10,11,14,30,31]. Our device performs favorably compared to prior NP-DBR VCSEL demonstrations, and the results are in line with prior curved mirror VCSEL demonstrations. However, we note that the threshold current density calculated from the threshold current divided by the current aperture area is not always an accurate metric, given that the injected current density is seldom uniform over the aperture and that the optical mode diameter is usually smaller than the current aperture diameter [9].

CW performance is limited by thermal rollover, which is caused by a higher than anticipated voltage. A high voltage is believed to be caused by incomplete activation of the TJ interface in the BTJ [5,32], which is a problem exacerbated by the thick n-GaN regrowth immediately following the BTJ etch. Additionally, the Mg doping within the p++-GaN of the BTJ is approximately [Mg] = 3 × 10^{20} cm^{-3} as measured using secondary ion mass spectrometry (SIMS), potentially leading to passivating Mg-H complexes at or near the TJ interface [33].

Figure 4a,b show the topside NFP images taken of the device below and above J_{th}. Above the threshold, a bright spot appears above the BTJ at the center of the lens that is approximately 2 μm wide. The spot diameter for a fundamental Gaussian beam at the concave mirror is calculated using the following equation [34]:

$$2\omega_{concave} = 2\sqrt{\frac{\lambda}{n\pi}\sqrt{\frac{L_{eff}^2 R^2}{L_{eff}R - L_{eff}^2}}} \tag{4}$$

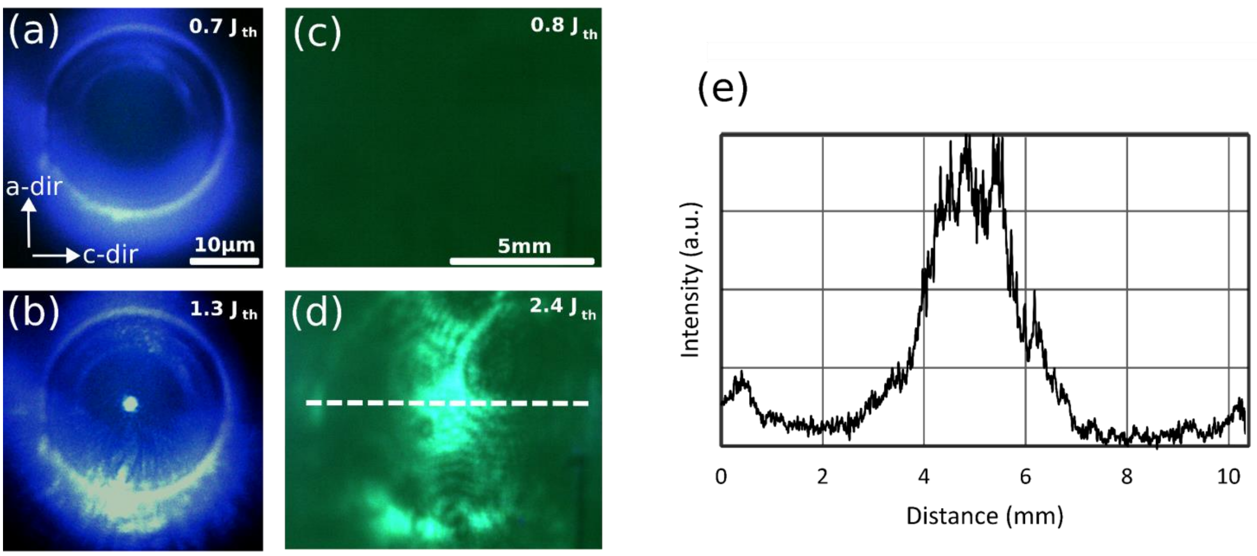

Figure 4. (**a**,**b**) Optical microscopic images of a 9 μm diameter aperture VCSEL below and above J_{th} (pulsed), respectively. (**c**,**d**) Captured images of the bottomside FFP of the same VCSEL below and above J_{th}, respectively. (**e**) Cross-sectional profile of the bottomside FFP above J_{th} taken along the c-direction.

For this design, the beam diameter was calculated to be 2.15 μm, which is in agreement with the observed experimental value.

Figure 4c,d show the fluorescent paper when illuminated through the bottomside of the VCSEL below J_{th} and above J_{th} at a bias of 10 mA. The rough SSP GaN substrate contributes to the significant scattering of the mode. However, a rough central lateral mode shape appears above the threshold and grows with the injected current. Figure 4e shows a 2D line scan of the mode, with a full width at half maximum (FWHM) of approximately 2.9 mm. The fluorescent paper was placed 16.5 mm away from the bottom of the 250 µm thick GaN substrate, leading to an extracted divergence half-angle, θ_{FWHM}, of 8.4°. This value is comparable to the theoretical $\theta_{FWHM} \approx 10°$ calculated using the following equation [27]:

$$\theta_{FWHM} = \sqrt{2ln2}\frac{\lambda}{\pi\omega_0} \tag{5}$$

Taking the radius of the spot observed in the topside NFP in Figure 4b and applying it to Equation (5) gives an expected topside θ_{FWHM} of 8.8°, which is in reasonable agreement with the bottomside value. The experimental top and bottom θ_{FWHM} values are in line with recent curved mirror cavity demonstrations, which reported divergence half-angles of 8.5° and 3.9° [11,35], but higher than recent planar cavity demonstrations, which reported divergence half-angles of 5.1° and 2.8° [3,36].

4. Conclusions

In summary, 60.5 λ cavity GaN-VCSELs utilizing a topside curved mirror, BTJ, and NP DBR were successfully fabricated. The peak output power for a 9 µm aperture under pulsed operation was 290 µW, with a J_{th} of 6.6 kA/cm^2 and η_d of 0.7%. Under CW operation, J_{th} increased to 7.3 kA/cm^2, η_d decreased to 0.4%, and the peak output power at rollover was 130 µW. The bottomside FFP images show that the divergence half-angle was approximately 8.4°.

Author Contributions: Conceptualization, N.C.P., R.A. and J.A.K.; data curation, N.C.P.; formal analysis, E.T.; funding acquisition, S.P.D. and S.N.; investigation, N.C.P., J.A.K. and J.B.; software, R.A. and S.G. All authors have read and agreed to the published version of the manuscript.

Funding: This work was funded by the Solid-State Lighting and Energy Electronics Center (SSLEEC) at UCSB.

Data Availability Statement: The results presented in this paper are not available publicly at this time but may be obtained from the authors upon reasonable request.

Acknowledgments: A portion of this work was carried out at the UCSB nanofabrication facility, the UCSB Materials Research Laboratory (NSF DMR 1720256), the NRI-MCDB Microscopy Facility (NSF DBR-1625770), and the California Nano System Institute (CNSI).

Conflicts of Interest: The authors declare no conflict of interest.

References

1. Michalzik, R. *VCSELs: Fundamentals, Technology and Applications of Vertical-Cavity Surface-Emitting Lasers*; Springer Series in Optical Sciences; Springer: Berlin/Heidelberg, Germany, 2013; ISBN 978-3-642-24985-3.
2. Hayashi, N.; Ogimoto, J.; Matsui, K.; Furuta, T.; Akagi, T.; Iwayama, S.; Takeuchi, T.; Kamiyama, S.; Iwaya, M.; Akasaki, I. A GaN-Based VCSEL with a Convex Structure for Optical Guiding. *Phys. Status Solidi A* **2018**, *215*, 1700648. [CrossRef]
3. Kuramoto, M.; Kobayashi, S.; Akagi, T.; Tazawa, K.; Tanaka, K.; Saito, T.; Takeuchi, T. High-Power GaN-Based Vertical-Cavity Surface-Emitting Lasers with AlInN/GaN Distributed Bragg Reflectors. *Appl. Sci.* **2019**, *9*, 416. [CrossRef]
4. Leonard, J.T.; Cohen, D.A.; Yonkee, B.P.; Farrell, R.M.; Margalith, T.; Lee, S.; DenBaars, S.P.; Speck, J.S.; Nakamura, S. Nonpolar III-Nitride Vertical-Cavity Surface-Emitting Lasers Incorporating an Ion Implanted Aperture. *Appl. Phys. Lett.* **2015**, *107*, 011102. [CrossRef]
5. Kearns, J.A.; Back, J.; Cohen, D.A.; DenBaars, S.P.; Nakamura, S. Demonstration of Blue Semipolar (2021) GaN-Based Vertical-Cavity Surface-Emitting Lasers. *Opt. Express* **2019**, *27*, 23707. [CrossRef]
6. ElAfandy, R.T.; Kang, J.-H.; Li, B.; Kim, T.K.; Kwak, J.S.; Han, J. Room-Temperature Operation of c-Plane GaN Vertical Cavity Surface Emitting Laser on Conductive Nanoporous Distributed Bragg Reflector. *Appl. Phys. Lett.* **2020**, *117*, 011101. [CrossRef]
7. Elafandy, R.T.; Kang, J.-H.; Mi, C.; Kim, T.K.; Kwak, J.S.; Han, J. Study and Application of Birefringent Nanoporous GaN in the Polarization Control of Blue Vertical-Cavity Surface-Emitting Lasers. *ACS Photonics* **2021**, *8*, 1041–1047. [CrossRef]
8. Kiyohara, K.; Odawara, M.; Takeuchi, T.; Kamiyama, S.; Iwaya, M.; Akasaki, I.; Saito, T. Room-Temperature Continuous-Wave Operations of GaN-Based Vertical-Cavity Surface-Emitting Lasers with Buried GaInN Tunnel Junctions. *Appl. Phys. Express* **2020**, *13*, 111003. [CrossRef]

9. Kearns, J.A.; Back, J.; Palmquist, N.C.; Cohen, D.A.; DenBaars, S.P.; Nakamura, S. Inhomogeneous Current Injection and Filamentary Lasing of Semipolar (2021¯) Blue GaN-Based Vertical-Cavity Surface-Emitting Lasers with Buried Tunnel Junctions. *Phys. Status Solidi (A)* **2019**, *217*, 1900718. [CrossRef]
10. Hamaguchi, T.; Tanaka, M.; Nakajima, H. A Review on the Latest Progress of Visible GaN-Based VCSELs with Lateral Confinement by Curved Dielectric DBR Reflector and Boron Ion Implantation. *Jpn. J. Appl. Phys.* **2019**, *58*, SC0806. [CrossRef]
11. Nakajima, H.; Hamaguchi, T.; Tanaka, M.; Ito, M.; Jyokawa, T.; Matou, T.; Hayashi, K.; Ohara, M.; Kobayashi, N.; Watanabe, H.; et al. Single Transverse Mode Operation of GaN-Based Vertical-Cavity Surface-Emitting Laser with Monolithically Incorporated Curved Mirror. *Appl. Phys. Express* **2019**, *12*, 084003. [CrossRef]
12. Hamaguchi, T.; Nakajima, H.; Tanaka, M.; Ito, M.; Ohara, M.; Jyoukawa, T.; Kobayashi, N.; Matou, T.; Hayashi, K.; Watanabe, H.; et al. Sub-Milliampere-Threshold Continuous Wave Operation of GaN-Based Vertical-Cavity Surface-Emitting Laser with Lateral Optical Confinement by Curved Mirror. *Appl. Phys. Express* **2019**, *12*, 044004. [CrossRef]
13. Ito, M.; Hamaguchi, T.; Makino, T.; Hayashi, K.; Kearns, J.; Ohara, M.; Kobayashi, N.; Nagane, S.; Sato, K.; Nakamura, Y.; et al. Highly Efficient Operation and Uniform Characteristics of Curved Mirror Vertical-Cavity Surface-Emitting Lasers. *Appl. Phys. Express* **2022**, *16*, 012006. [CrossRef]
14. Hamaguchi, T.; Tanaka, M.; Mitomo, J.; Nakajima, H.; Ito, M.; Ohara, M.; Kobayashi, N.; Fujii, K.; Watanabe, H.; Satou, S.; et al. Lateral Optical Confinement of GaN-Based VCSEL Using an Atomically Smooth Monolithic Curved Mirror. *Sci. Rep.* **2018**, *8*, 10350. [CrossRef]
15. Kogelnik, H.; Li, T. Laser Beams and Resonators. *Appl. Opt. AO* **1966**, *5*, 1550–1567. [CrossRef]
16. Hwang, D.; Mughal, A.; Wong, M.; Alhassan, A.; Nakamura, S.; Denbaars, S. Micro-Light-Emitting Diodes with III–Nitride Tunnel Junction Contacts Grown by Metalorganic Chemical Vapor Deposition. *Appl. Phys. Express* **2018**, *11*, 012102. [CrossRef]
17. Wong, M.S.; Palmquist, N.C.; Jiang, J.; Chan, P.; Lee, C.; Li, P.; Kang, J.H.; Baek, Y.H.; Kim, C.H.; Cohen, D.A.; et al. Effects of Activation Method and Temperature to III-Nitride Micro-Light-Emitting Diodes with Tunnel Junction Contacts Grown by Metalorganic Chemical Vapor Deposition. *Appl. Phys. Lett.* **2021**, *119*, 202102. [CrossRef]
18. Kioupakis, E.; Rinke, P.; Van de Walle, C.G. Determination of Internal Loss in Nitride Lasers from First Principles. *Appl. Phys. Express* **2010**, *3*, 082101. [CrossRef]
19. Nussbaum, P.; Völkel, R.; Herzig, H.P.; Eisner, M.; Haselbeck, S. Design, Fabrication and Testing of Microlens Arrays for Sensors and Microsystems. *Pure Appl. Opt.* **1997**, *6*, 617–636. [CrossRef]
20. Kuwano, Y.; Kaga, M.; Morita, T.; Yamashita, K.; Yagi, K.; Iwaya, M.; Takeuchi, T.; Kamiyama, S.; Akasaki, I. Lateral Hydrogen Diffusion at P-GaN Layers in Nitride-Based Light Emitting Diodes with Tunnel Junctions. *Jpn. J. Appl. Phys.* **2013**, *52*, 08JK12. [CrossRef]
21. Palmquist, N.C.; Anderson, R.; Kearns, J.A.; Back, J.; Trageser, E.; Gee, S.; Denbaars, S.P.; Nakamura, S. Continuous-Wave Operation of Long-Cavity m-Plane GaN-Based Vertical-Cavity Surface-Emitting Lasers with a Topside Curved Mirror and Nanoporous GaN DBR. In Proceedings of the Gallium Nitride Materials and Devices XVIII, San Francisco, CA, USA, 15 March 2023; Volume 12421, pp. 127–135.
22. Wong, M.S.; Hwang, D.; Alhassan, A.I.; Lee, C.; Ley, R.; Nakamura, S.; DenBaars, S.P. High Efficiency of III-Nitride Micro-Light-Emitting Diodes by Sidewall Passivation Using Atomic Layer Deposition. *Opt. Express OE* **2018**, *26*, 21324–21331. [CrossRef]
23. Zhang, C.; Park, S.H.; Chen, D.; Lin, D.-W.; Xiong, W.; Kuo, H.-C.; Lin, C.-F.; Cao, H.; Han, J. Mesoporous GaN for Photonic Engineering—Highly Reflective GaN Mirrors as an Example. *ACS Photonics* **2015**, *2*, 980–986. [CrossRef]
24. Braun, M.M.; Pilon, L. Effective Optical Properties of Non-Absorbing Nanoporous Thin Films. *Thin Solid Films* **2006**, *496*, 505–514. [CrossRef]
25. Anderson, R.; Cohen, D.; Zhang, H.; Trageser, E.; Palmquist, N.; Nakamura, S.; DenBaars, S. Nano-Porous GaN Cladding and Scattering Loss in Edge Emitting Laser Diodes. *Opt. Express OE* **2022**, *30*, 2759–2767. [CrossRef]
26. Leonard, J.T.; Young, E.C.; Yonkee, B.P.; Cohen, D.A.; Margalith, T.; DenBaars, S.P.; Speck, J.S.; Nakamura, S. Demonstration of a III-Nitride Vertical-Cavity Surface-Emitting Laser with a III-Nitride Tunnel Junction Intracavity Contact. *Appl. Phys. Lett.* **2015**, *107*, 091105. [CrossRef]
27. Yariv, A. *Optical Electronics*, 3rd ed.; Saunders College Publishing: Philadelphia, PA, USA, 1991; ISBN 978-1-60049-013-2.
28. Mishkat-Ul-Masabih, S.M.; Aragon, A.A.; Monavarian, M.; Luk, T.S.; Feezell, D.F. Electrically Injected Nonpolar GaN-Based VCSELs with Lattice-Matched Nanoporous Distributed Bragg Reflector Mirrors. *Appl. Phys. Express* **2019**, *12*, 036504. [CrossRef]
29. Ke, Y.; Wang, C.-J.; Shiu, G.-Y.; Chen, Y.-Y.; Lin, Y.-S.; Chen, H.; Han, J.; Lin, C.-F. Polarization Properties of InGaN Vertical-Cavity Surface-Emitting Laser with Pipe Distributed Bragg Reflector. *IEEE Trans. Electron. Devices* **2022**, *69*, 201–204. [CrossRef]
30. Hamaguchi, T.; Hoshina, Y.; Hayashi, K.; Tanaka, M.; Ito, M.; Ohara, M.; Jyoukawa, T.; Kobayashi, N.; Watanabe, H.; Yokozeki, M.; et al. Room-Temperature Continuous-Wave Operation of Green Vertical-Cavity Surface-Emitting Lasers with a Curved Mirror Fabricated on (2021) Semi-Polar GaN. *Appl. Phys. Express* **2020**, *13*, 041002. [CrossRef]
31. Kearns, J.; Hamaguchi, T.; Hayashi, K.; Ohara, M.; Makino, T.; Ito, M.; Kobayashi, N.; Jyoukawa, T.; Nakayama, E.; Nagane, S.; et al. Longitudinal Mode Control in Long Cavity VCSELs with a Curved Mirror. *Appl. Phys. Express* **2022**, *15*, 072009. [CrossRef]
32. Leonard, J.T.; Yonkee, B.P.; Cohen, D.A.; Megalini, L.; Lee, S.; Speck, J.S.; DenBaars, S.P.; Nakamura, S. Nonpolar III-Nitride Vertical-Cavity Surface-Emitting Laser with a Photoelectrochemically Etched Air-Gap Aperture. *Appl. Phys. Lett.* **2016**, *108*, 031111. [CrossRef]

33. Castiglia, A.; Carlin, J.-F.; Grandjean, N. Role of Stable and Metastable Mg–H Complexes in p-Type GaN for Cw Blue Laser Diodes. *Appl. Phys. Lett.* **2011**, *98*, 213505. [CrossRef]
34. Aldaz, R.I.; Wiemer, M.W.; Miller, D.A.B.; Harris, J.S. Monolithically-Integrated Long Vertical Cavity Surface Emitting Laser Incorporating a Concave Micromirror on a Glass Substrate. *Opt. Express OE* **2004**, *12*, 3967–3971. [CrossRef] [PubMed]
35. Hayashi, K.; Hamaguchi, T.; Kearns, J.A.; Kobayashi, N.; Ohara, M.; Makino, T.; Nagane, S.; Sato, K.; Nakamura, Y.; Hoshina, Y.; et al. Narrow Emission of Blue GaN-Based Vertical-Cavity Surface-Emitting Lasers With a Curved Mirror. *IEEE Photonics J.* **2022**, *14*, 1–5. [CrossRef]
36. Kuramoto, M.; Kobayashi, S.; Tazawa, K.; Tanaka, K.; Akagi, T.; Saito, T. In-Phase Supermode Operation in GaN-Based Vertical-Cavity Surface-Emitting Laser. *Appl. Phys. Lett.* **2019**, *115*, 041101. [CrossRef]